Bulletin of the JSME Vol.000,No.00,2014
Mechanical Engineering Journal

Laminar-turbulent transition of an inlet boundary layer in a circular pipe induced by periodic injection (Turbulence within isolated turbulent patches and its growth mechanism)

Masashi ICHIMIYA*, Hayato MATSUDAIRA** and Hayato FUJIMURA**
* Institute of Technology and Science, The University of Tokushima
2-1 Minami-Josanjima-cho, Tokushima-shi, Tokushima, 770-8506, Japan
E-mail: ichimiya@tokushima-u.ac.jp
** Graduate School, The University of Tokushima

Abstract
The laminar-turbulent transition of a boundary layer induced by a jet injection in the inlet region of a circular pipe was experimentally investigated. The jet was periodically injected radially from a small hole in the inlet region into the pipe flow. Axial velocity was measured by a hot-wire anemometer. The turbulence induced by the jet within the boundary layer developed into turbulent patches which grew in the axial, circumferential and radial directions downstream. Turbulent fluctuations within the patch were maximum a little inside the leading edge in the axial direction and slightly inside the circumferential interface in the circumferential direction. Non-turbulent fluid was entrained into the patch through the leading and trailing edges. This was the main reason for the axial growth of the patch downstream. If the entrainment is suppressed, the axial growth is inhibited. The axial distance between the leading edge and maximum fluctuation position varied little downstream. On the other hand, the distance between the maximum fluctuation position and the trailing edge increased downstream due to the increase in the entrainment of non-turbulent fluid across the trailing edge.

Keywords : Pipe Flow, Transition, Boundary Layer, Turbulence, Inlet Region, Isolated Turbulent Patch, Turbulent Spot

1. Introduction

Fully developed laminar pipe flow (Hagen-Poiseuille; HP flow) has been shown to be stable in infinitesimal disturbances from theoretical and experimental studies (Kerswell, 2005)(Eckhardt, et al., 2007)(Eckhardt, 2008)(Willis, et al., 2008). As is well known, however, if the Reynolds number exceeds a threshold level (1800－2300), isolated turbulent patches (turbulent puffs or slugs) originate intermittently. They occupy the whole cross section and their axial length grows downstream, then the flow always shows turbulence finally. The contradiction between the above fact and the linear stability theory is attributed to an ignorance of two factors in the theory; finite amplitude disturbance and upstream inlet (entrance) region. The latter has been shown to be unstable in finite Reynolds number. Therefore, the role that the inlet region plays in the laminar-turbulent transition is significant, and is expected to be elucidated. At present, however, investigations about the inlet flow are less than those of HP flow.

The present authors have conducted experiments that introduced a disturbance to the inlet laminar flow, studied the steady turbulent region formed downstream of three-dimensional single roughness element on the wall, and revealed its properties (Ichimiya, et al., 2007). Next, isolated turbulent patches were generated by a jet injected perpendicularly to the pipe flow from a hole in the wall (Ichimiya, et al., 2011, 2013). In the experiments, the threshold flow rate of the jet to create the turbulence differed from that of the HP flow. In addition, effects of the jet flow rate and injection frequency on the extent of and velocity fluctuation within the turbulent patches were clarified (Ichimiya, et al., 2011). Moreover, the form, relationship between the surrounding laminar boundary layer and growth of the patches were

Received 16 August 2013 (No.xx-xxxx)
[DOI: 00.0000/ABCDE0.0000000]

compared with turbulent puffs and slugs in the HP flow and the turbulent spots in the flat-plate boundary layer (Ichimiya, et al., 2013). However, details of the turbulence inside and growth mechanism of the patches have not been clarified.

In the present paper, velocity deviation from an ensemble-averaged velocity, i.e., irregularly fluctuating velocity is obtained, then the turbulence inside the turbulent patches is examined. In addition to examine the growth mechanism of the patches, relative streamlines were obtained with respect to their leading and trailing edges along with the conditionally-averaged velocity based on the condition of turbulence/non-turbulence. From them, the way in which the outside non-turbulent fluid is entrained into the patches from both edges and becomes turbulent was clarified. Differences in the turbulent patches from turbulent puffs or slugs in the HP flow and the turbulent spots in the flat-plate boundary layer were also examined.

2. Experimental apparatus and methods

The experimental apparatus is the same one used in the previous paper (Ichimiya, et al., 2011, 2013). A plexiglas pipe with a diameter, $D = 2a$, of 60 mm and a total length of approximately 6.2 m (= $104D$) was used in the experiments. A fan downstream of the pipe sucked air into the pipe. Six pipes, each 1 m in length, are connected smoothly. The axial velocity was axisymmetric. For the convenience of the reader, the coordinate system and flow field are reproduced in Fig. 1. As a point disturbance, a single jet flow was injected perpendicularly to the main flow through a 2-mm diameter hole 107 mm downstream of the coordinate origin, as shown in Fig. 1.

In the present study, in order to inject the jet periodically, air emitted from an air pump is led to a solenoid valve. In the control signal of the solenoid valve, periodically generated rectangular voltage from a photo-interrupter is led to the valve. The injection duration is 0.1 seconds. The threshold jet flow rate for generating the isolated turbulent patch decreases with the duration and it finally saturates (Ichimiya, et al., 2011). Therefore, too long duration was avoided. The interval (non-injection duration), t_{j2}, is 0.3 or 0.7 seconds; therefore, the combination time of jet flow injection and non-injection, T_j, is 0.4 or 0.8 seconds. For measurements not too far downstream from the jet hole $(x-x_j)/D \leqq 19.2$, the non-injection duration is 0.3s. On the other hand, for downstream $26.1 \leqq (x-x_j)/D$, since the turbulent patch elongates (Ichimiya, et al., 2013), the non-injection duration is extended to 0.7s in order to keep adjacent patches from merging. As seen in Fig. 2, except for $(x-x_j)/D = 42.7$ (Fig. 2 (*i*)), the non-turbulent region encompasses the turbulent patches.

The Reynolds number based on the pipe diameter and the velocity averaged over the cross section, U_a, is kept at 10000 ($U_a \simeq 2.5$ m/s) as in the previous report (Ichimiya, et al., 2013). The jet flow rate was set to 6.3×10^{-6} m^3/s (jet speed $v_j = 2.0$ m/s) which sufficiently exceeds the threshold value to generate the turbulent patch at $Re = 10000$ (Ichimiya, et al., 2011). If the jet flow rate increases, the velocity fluctuation within the patch does not change and the duration of the turbulent patch increases (Ichimiya, et al., 2011). Therefore, too much flow rate was avoided. Without the jet, the inlet region continues over the whole pipe length (Ichimiya, et al., 2011).

A single hot-wire probe with a tungsten sensing element 5 μm in diameter and 1 mm in length was used for axial velocity measurements. This probe senses not only the axial but also the radial velocity component. In preliminary experiments with X-wire probe, the radial velocity component was smaller than the axial one. Therefore, as well as references with single-wire probes (Eliahou, et al., 1998)(Han, et al., 2000)(Durst, et al., 2006)(Nishi, et al., 2008), only

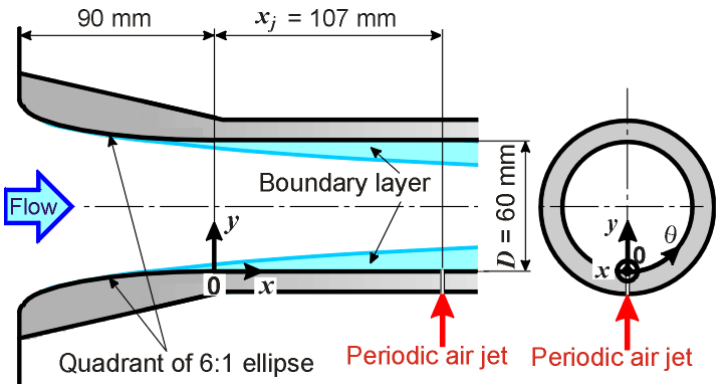

Fig. 1 Coordinate system and air jet

axial component was regarded to have been measured. Output voltage from the hot wire had been digitized at a 10 kHz sampling frequency and a 52-second sampling period. An ensemble averaging based on the output voltage from the photointerrupter was performed. The ensemble-averaged data is a function of the elapsed time from the jet injection. The 52-second sampling period corresponds to 130 and 65 times of the ensemble average in the region of $(x-x_j)/D \leqq 19.2$ (T_j = 0.4s) and $26.1 \leqq (x-x_j)/D$ (T_j = 0.8s), respectively.

Results are shown here in the axial stations within $(x-x_j)/D$ = 2.5, 3.5, 9.4, 14.9, 19.2, 26.1, 31.6, 35.8 and 42.7. When the jet is injected, these stations are still within the inlet region (Ichimiya, et al., 2013). A pipe of 150 mm in length including the jet injection hole is adapted to rotate around its center axis. That makes it possible to select the desired circumferential measurement position, θ, relatively to the hole. Only the station of $(x-x_j)/D$ = 9.4 in both ranges of $-180° \leqq \theta \leqq 0°$ and $0° \leqq \theta \leqq 180°$, were measured. Since the symmetry with respect to the center position $\theta = 0^\circ$ was good (Ichimiya, et al., 2013), in the other stations only a region of $0° \leqq \theta \leqq 180°$ was measured. Forty-three radial positions were measured in the region of 0.2 mm $\leqq y \leqq$ 30 mm.

To distinguish the flow as laminar or turbulent, in the present experiment a one-order time derivative of axial fluctuating velocity was compared with a constant threshold value which has been judged as valid from many comparisons between the discrimination results and instantaneous velocity signals (Ichimiya, et al., 2011, 2013).

3. Results and discussion

3.1 Turbulence within turbulent patch

In this section, the turbulence i.e., the irregularly fluctuating velocity within the turbulent patch is examined. Figure 2 shows contour maps of the root mean square value of the fluctuating velocity on diametrical planes which pass through the jet hole (θ = 0°, y = 0), the pipe center axis and the wall of θ = 180°. The method for estimating the value is as follows. The instantaneous velocity at an instantaneous time $\tilde{t}$ is written as $\tilde{u}(\tilde{t}) = U + u(\tilde{t})$, where U means the time-averaged velocity. The instantaneous time in the k-th ensemble whose phase, i.e., the elapsed time from the jet injection within the ensemble, was equal to the time, t, in the first ensemble is t + (k-1)T_j. Therefore, the ensemble-averaged velocity at elapsed time, t, from the jet injection time is expressed as

$$<\tilde{u}>(t) = <U+u>(t) = \frac{1}{n}\sum_{k=1}^{n}\left[U + u\left(t+(k-1)T_j\right)\right] = \frac{1}{n}\sum_{k=1}^{n}\left[U+u(t_k)\right] = U + \frac{1}{n}\sum_{k=1}^{n}u(t_k) = U + <u>(t) \tag{1}$$

Where n means a sampled frequency number, i.e., number of the ensemble averaging. The starting and terminal values of a summation are omitted from the summation sign below. The difference of $\tilde{u}(\tilde{t})$ and $<\tilde{u}>(t)$, i.e., irregularly fluctuating velocity $\hat{u}(\tilde{t})$ is squared first, then ensemble-averaged. The square root of that is taken finally, and called the root mean square value, u':

$$u'^2(t) \equiv <\hat{u}^2>(t) = <[\tilde{u}(\tilde{t}) - <\tilde{u}>(t)]^2>(t) = <[u(\tilde{t}) - <u>(t)]^2>(t) = <u^2>(t) - <u>^2(t) \tag{2}$$

The familiar root mean square value means: The difference, $u(\tilde{t})$, between an instantaneous velocity and time-averaged velocity is squared, time-averaged again, and the square root is taken finally. In the present paper, not the time-averaged but the ensemble-averaged velocity is called a root mean square value.

In Fig. 2, the root mean square value is normalized by the time-averaged velocity at the edge of the boundary layer.

The numerical value in the ordinate is a height measured from the surface of the jet-hole side ($\theta = 0°$) wall normalized

by the pipe radius. That in the abscissa is a elapsed time normalized by cross-sectional average velocity and the pipe

diameter, $T = U_a(t + nT_j) / D$ (n is an integer larger than or equal to zero). The left (small T) or right (large T) sides

correspond to the leading or trailing edge sides of the turbulent patch, respectively. As a guide for the patch form,

contour lines of a half-intermittency ($<I> = 0.5$) are also drawn in white lines. The method to estimate the intermittency

factor is described in the previous report (Ichimiya, et al., 2013). In the contour lines of the half-intermittency, the ones

which face the downstream and upstream sides are called the leading and trailing edges, respectively. Moreover, the

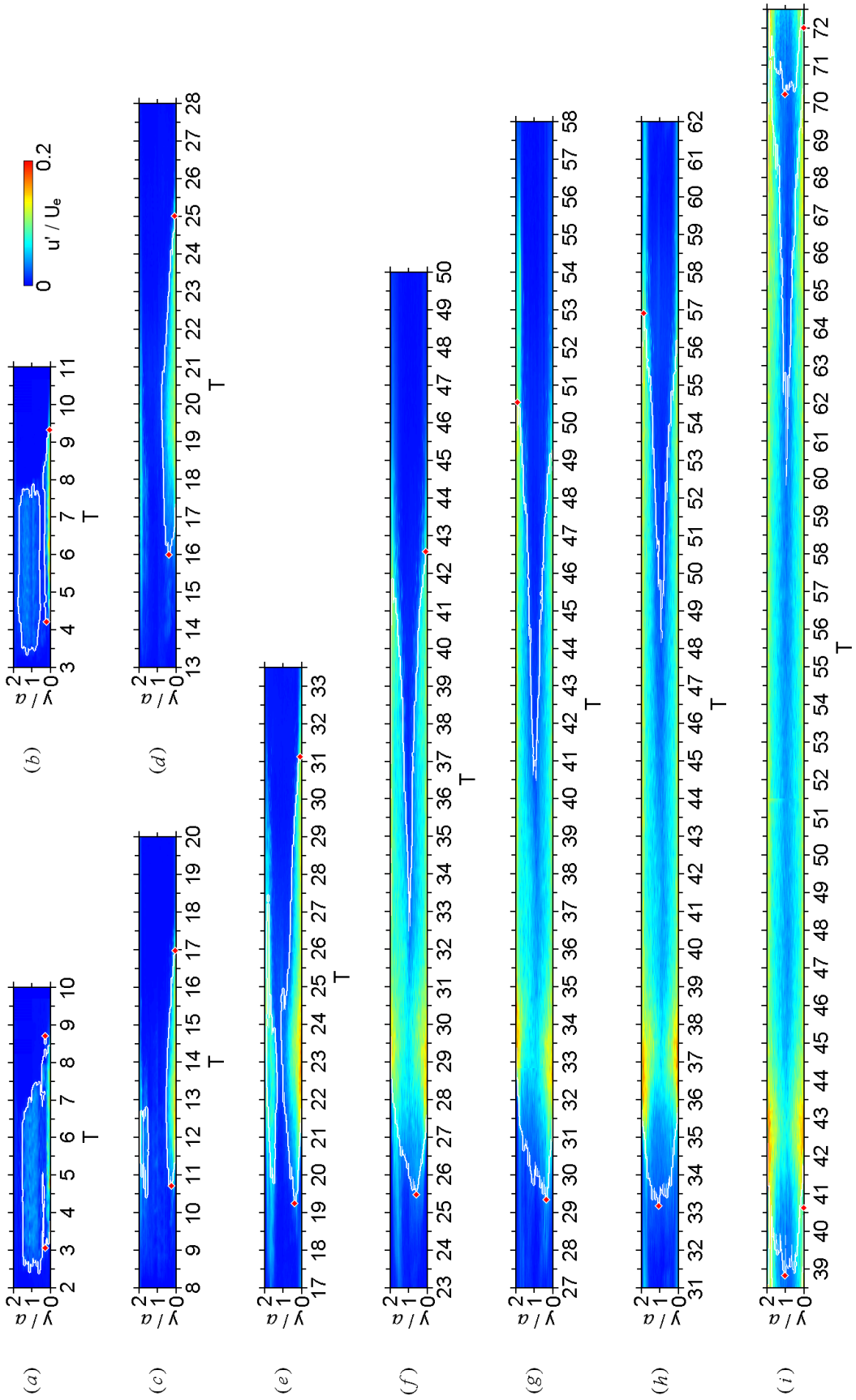

Fig. 2 Contour maps of fluctuating velocity on diametrical plane. (*a*) $(x-x_j)/D = 2.5$; (*b*) $(x-x_j)/D = 3.5$; (*c*) $(x-x_j)/D = 9.4$; (*d*) $(x-x_j)/D = 14.9$; (*e*) $(x-x_j)/D = 19.2$; (*f*) $(x-x_j)/D = 26.1$; (*g*) $(x-x_j)/D = 31.6$; (*h*) $(x-x_j)/D = 35.8$; (*i*) $(x-x_j)/D = 42.7$. white line, $\langle I \rangle = 0.5$.

most downstream position (the smallest T) of the leading edge is called the most downstream leading edge, T_l, here. On the other hand, the most upstream position (the largest T) of the trailing edge is called the most upstream trailing edge, T_t, here. The most downstream leading and most upstream trailing edges are shown as red asterisks in Fig. 2.

At $(x-x_j)/D = 2.5$ (Fig. 2(a)), the patch is beginning to separate into the pipe wall ($\theta = 0°$) part and upper part. As discussed previously in detail (Ichimiya, et al., 2013), the upper patch is judged to be the jet itself which is injected from the jet hole perpendicularly to the pipe flow. Since the jet rises and enters the pipe core without velocity gradient, it is expected to disappear. On the other hand, the turbulent patch in the wall side is considered to have been induced by the jet. Since the wall-side patch exists in the boundary layer as the flat- plate turbulent spot, it grows.

As described in the intermittency contour maps in the previous paper (Ichimiya, et al., 2013), in the upstream stations, $(x-x_j)/D \leqq 19.2$ (Fig. 2(a)~(e)), the form of the patch is the turbulent spot type, i.e., the height of the patch is almost the same as the local boundary layer thickness and contacts with the free stream. On the other hand, in the downstream stations, $26.1 \leqq (x-x_j)/D$ (Fig. 2(f)~(i)), the form is the turbulent slug type, i.e., the patch covers a cross section totally. The fluctuating velocity is at maximum at the position about 4 inside of the turbulent patch from its leading edge and near the wall. In the turbulent slugs in the HP flow, the fluctuation is larger at the region near the leading or trailing edges than a position well inside the slugs (Wygnanski and Champagne, 1973). On the other hand, in the turbulent spots, the fluctuation is larger at a position slightly inside the leading edge (Glezer, et al., 1989)(Makita and Nishizawa, 1998). The property that the fluctuation is large at a position slightly inside the leading edge in many turbulent patches is similar to flat-plate boundary-layer turbulent spots. On the other hand, in the region of $26.1 \leqq (x-x_j)/D$, the patch is similar to turbulent slugs.

Wygnanski et al. showed that the fluctuating velocity in the fluid taken into the slugs in the HP flow is larger than the inside of the slugs (Wygnanski and Champagne, 1973). They showed that the evidence for this result was an increase in fluctuating velocity just before the breakdown of the laminar flow. They also found that the main reason for the large fluctuating velocity was an inflection point in the mean velocity profile there. The non-turbulent fluid entrained in the present turbulent patch will be shown in §3.2. Though a figure is not shown, around the leading and trailing edges of the present turbulent patch, the point of inflection exists in the distributions of an ensemble-averaged velocity, $U + \langle u \rangle$, thus suggesting instability. For this reason, the position where the fluctuating velocity within the patch is large is considered to be where the non-turbulent fluid entrainment became very turbulent because of this instability. The fact that the velocity fluctuation is large near the leading or trailing edges means that when the patch grows axially, the action involving non-turbulent fluid within a boundary layer (mean vorticity, $\partial U / \partial y$, is large near the wall) is considerable. In §3.2, the relation between the non-turbulent fluid entrainment and growth of the patch is also discussed.

To investigate the relationship between the range of the patch and active fluctuation, three positions are shown in Fig. 3(a); the most downstream leading edge, T_l, the maximum fluctuating position in the whole (T, y) positions, T_m, and the most upstream trailing edge, T_t. The three positions are approximated by power functions except for $(x-x_j)/D \leqq 6$ of T_t, and are shown by three solid lines in Fig. 3(a). As previously shown (Ichimiya, et al., 2013), in the region of $(x-x_j)/D \leqq 6$, since this region is immediately after the jet injection, the tendency of the trailing edge significantly differs from others. The distance between the most downstream leading edge and the maximum fluctuating position is almost constant, approximately 4, irrespective of the patch type. On the other hand, the distance between the maximum fluctuating position and the most upstream trailing edge increases greatly downstream as well as turbulent spots

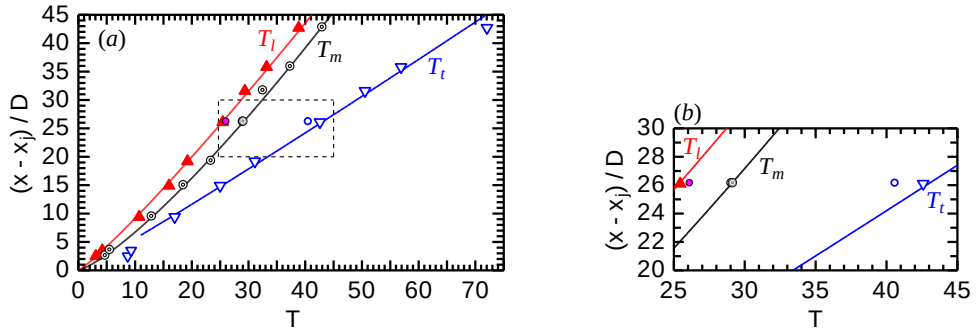

Fig. 3 Downstream variation of most downstream leading edge (▲), maximum fluctuating position (◎) and most upstream trailing edge (▽).

(Glezer, et al., 1989). The reason for the increase in the turbulent spot has been explained for the wave packet behind, i.e., upstream of the spots a breakdown occurs and becomes turbulent (Glezer, et al., 1989). For the present patch, little is known about the breakdown of such a wave packet. The reason for the present increase in the distance can be traced to the fact that the non-turbulent fluid taken from the trailing edge is larger than that of the leading edge. Details are considered in §3.2. The distance was able to be approximated by an exponential function, $T_t - T_m = 2.57\exp[0.0580(x - x_j)/D]$, or by a power function, $T_t - T_m = 0.197[(x - x_j)/D]^{1.29}$, though the latter function coincides slightly better with the experimental results. This means that if $(x - x_j)/D$ is denoted by ξ, the spatial derivative $d(T_t - T_m)/d\xi$ is approximated as the power function, $1.29(T_t - T_m)/\xi$, better than the exponential function, $0.0580(T_t - T_m)$. The distance may be influenced by the turbulent patch itself anyway. At $(x - x_j)/D = 26.1$, the red closed circle and the blue open circle are also plotted. A magnified view of this area (dashed frame in Fig. 3(*a*)) is shown in Fig. 3(*b*). This is T_l and T_t with the smaller jet non-injection interval, 0.3 second. In this condition the patch is slightly shorter due to the reduced non-turbulent fluid taken from the trailing edge. This condition is also discussed in §3.2.

The irregularly fluctuating velocity is investigated quantitatively, here. In Fig. 4, the variation of u' as a function of T is drawn in black lines (almost coincide with green and blue lines within and out of the patch, respectively) at the height of the maximum of u' in the whole (T, y) positions in $\theta = 0°$ at respective $(x - x_j)/D$. Moreover, in each T, turbulent fluctuating velocity, u_T', conditioned by turbulence from the turbulent sample is drawn by green lines. Additionally, non-turbulent fluctuating velocity, u_N', conditioned by non-turbulence from the non-turbulent sample, is indicated by blue lines. These fluctuating velocities are obtained as follows.

In the conditional ensemble averaging only turbulent or non-turbulent data are ensemble-averaged at each t. Turbulent and non-turbulent ensemble-averaged mean velocities, $<\tilde{u}>_T(t)$ and $<\tilde{u}>_N(t)$ are given below, respectively:

$$\langle\tilde{u}\rangle_T(t) = \frac{\Sigma\, I(t_k)\tilde{u}(t_k)}{I_\Sigma} = \frac{\Sigma\, I(t_k)U}{I_\Sigma} + \frac{\Sigma\, I(t_k)u(t_k)}{I_\Sigma} = U + \langle u\rangle_T(t) \equiv U + u_{ET}(t) \tag{3}$$

$$\langle\tilde{u}\rangle_N(t) = \frac{\Sigma\, [1 - I(t_k)]\tilde{u}(t_k)}{n - I_\Sigma} = \frac{\Sigma\, [1 - I(t_k)]U}{n - I_\Sigma} + \frac{\Sigma\, [1 - I(t_k)]u(t_k)}{n - I_\Sigma} = U + \langle u\rangle_N(t) \equiv U + u_{EN}(t) \tag{4}$$

Where I_Σ means a number of turbulent ensemble, $\Sigma I(t_k)$. Variations with a phase in above two fluctuating velocities and non-conditioned ensemble-averaged velocity, $u_{ET}(t)$, $u_{EN}(t)$ and $< u >(t)$, are related with the following equation:

$$< u >(t) = < I >(t)\, u_{ET}(t) + [\, 1 - < I >(t)\,]\, u_{EN}(t) \tag{5}$$

Deviations from the turbulent or non-turbulent ensemble-averaged velocity are squared first, then ensemble-averaged with respect to turbulent or non-turbulent fluid again. We next obtain the following quantities, respectively:

$$u_T'^2(t) \equiv \left\langle [u(\tilde{t}) - u_{ET}(t)]^2 \right\rangle_T(t) = \frac{\Sigma\, I(t_k)[u(t_k) - u_{ET}(t)]^2}{I_\Sigma} = \frac{\Sigma\, I(t_k)u(t_k)^2}{I_\Sigma} - u_{ET}^2(t) \tag{6}$$

$$u_N'^2(t) \equiv \left\langle [u(\tilde{t}) - u_{EN}(t)]^2 \right\rangle_N(t) = \frac{\Sigma\, [1 - I(t_k)][u(t_k) - u_{EN}(t)]^2}{n - I_\Sigma} = \frac{\Sigma\, [1 - I(t_k)]u(t_k)^2}{n - I_\Sigma} - u_{EN}^2(t) \tag{7}$$

Both conditional fluctuations are related with the non-conditional fluctuations as follows:

$$u'^2(t) = <I>(t)\, u_T'^2(t) + [1 - <I>(t)]\, u_N'^2(t) + <I>(t)\, [1 - <I>(t)]\, [u_{ET}(t) - u_{EN}(t)]^2 \tag{8}$$

Although these three quantities are functions of t, they are shown in Fig. 4 as a function of $T = U_a(t + nT_j)/D$. Where the turbulent and non-turbulent averages, u_T' and u_N', are drawn in the region of $0.05 \leqq < I > \text{ and } < I > \leqq 0.95$,

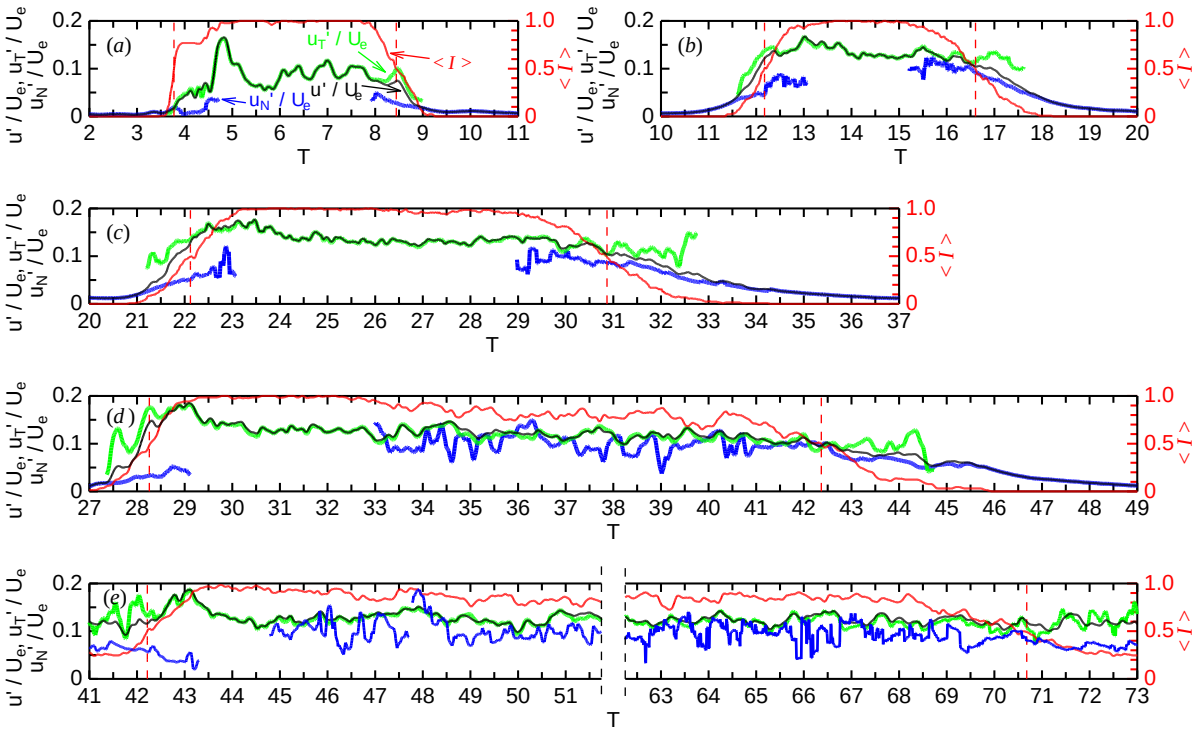

Fig. 4 Ensemble-averaged fluctuating velocities (left axis and black, green and blue lines) and intermittency factor (right axis and red solid line). $\theta = 0^\circ$. (*a*) $(x-x_j)/D = 2.5$, $y/a = 0.07$; (*b*) $(x-x_j)/D = 9.4$, $y/a = 0.03$; (*c*) $(x-x_j)/D = 19.2$, $y/a = 0.05$; (*d*) $(x-x_j)/D = 26.1$, $y/a = 0.04$; (*e*) $(x-x_j)/D = 42.7$, $y/a = 0.03$.

respectively.

In Fig. 4, the intermittency factor is also shown in red solid lines. Moreover, the leading and trailing edges at the height from the wall are indicated of T where the intermittency factor equals 0.5, and they are also shown by red vertical dashed lines. Note the most downstream leading and most upstream trailing edges in each $(x-x_j)/D$ are located farther downstream and upstream from the position of the half-intermittency, respectively. In $(x-x_j)/D = 42.7$ (Fig. 4(*e*)), the central part of the turbulent patch is omitted. The non-conditional fluctuating velocity, *u*', becomes the maximum inside the patch approximately 1 from the leading edge. For this reason, the increase in the fluctuating velocity near the leading edge is steep, on the other hand, the decrease near the trailing edge is gradual. This situation does not change upstream or downstream. That is, even after the form of the turbulent patch changed to the turbulent-slug type, the change of fluctuating velocity is clearer in the leading edge, and less clear in the trailing edge like the flat-plate turbulent spots. In addition, at $(x-x_j)/D = 42.7$ (Fig. 4(*e*)), *u*' is seldom decreasing in the trailing edge. The reason is, since the turbulent patch is quite longer there as shown in Fig. 2(*i*) and the interval between two adjacent patches is shorter, the next turbulent patch arrives there while the previous patch is passing.

The relationship between the non-conditional and conditional fluctuating velocities is explained for $(x-x_j)/D = 19.2$ (Fig. 4(*c*)) as an example. In the region $T < 21$, the outside of the patch, the non-conditional and non-turbulent values well coincide since the intermittency factor equals zero. As T increases and the leading edge of the patch approaches, the intermittency factor begins to increase, the non-conditional value thus begins to separate from the non-turbulent value and approaches the turbulent value. The turbulent value is larger than the non-turbulent value. Within the patch, since the intermittency factor is approximately unity, the non-conditional value almost coincides with the turbulent value. At the trailing edge, unlike the leading edge, the non-conditional value separates from the turbulent value and approaches the non-turbulent value. In the region $33 < T$, the outside of the patch, the non-conditional value well coincides with the non-turbulent value.

In this research, the ensemble averaging is based on the elapsed time, t, from the start time of the jet injection; thus the passage time of the leading edge in the respective patches does not align nor does that of the trailing edge. In this case, when the patch comes, the velocity variation with time is large near the wall since the velocity difference in the turbulent and non-turbulent flows is large there. Therefore, at the leading edge where the interface is definite, this large velocity difference will contribute to the fluctuation from the ensemble-averaged velocity. This means that if the difference of $u_{ET}(t)$ and $u_{EN}(t)$ in Eq. (8) is large, the non-conditional fluctuating velocity, $u'(t)$, becomes larger than the turbulent-conditional one, $u_T'(t)$. In order to confirm whether such a "fake" fluctuation has arisen, both quantities were compared in Fig. 4. Then, one can readily see that, at the leading and trailing edges, the almost turbulent-conditional velocity is larger than the non-conditional one. Therefore, the increase of the non-conditional fluctuation is mainly

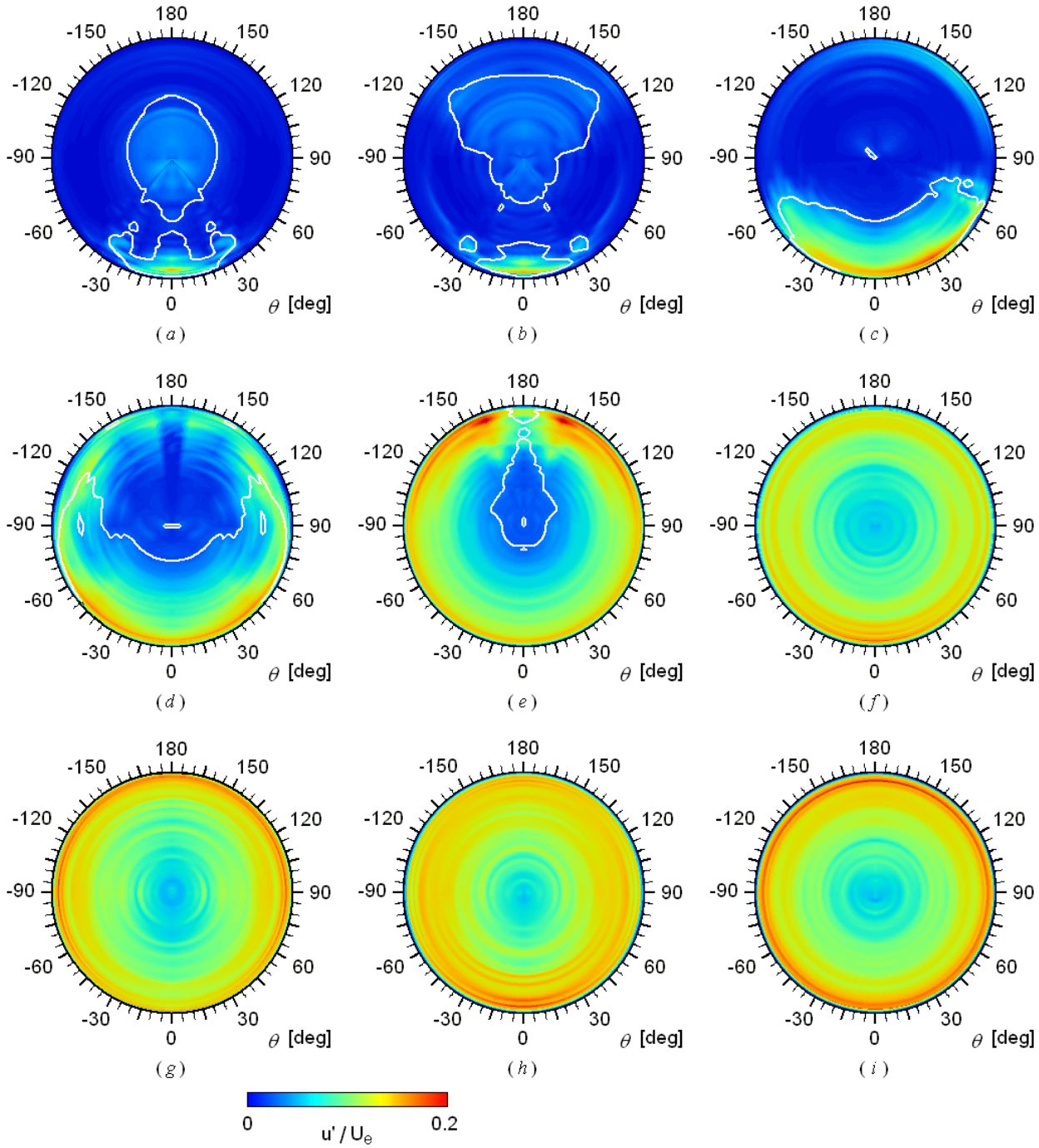

Fig. 5 Contour maps of fluctuating velocity on cross sections. (*a*) $(x-x_j)/D = 2.5$, $T = 4.8$; (*b*) $(x-x_j)/D = 3.5$, $T = 5.6$; (*c*) $(x-x_j)/D = 9.4$, $T = 13.8$; (*d*) $(x-x_j)/D = 14.9$, $T = 19.0$; (*e*) $(x-x_j)/D = 19.2$, $T = 24.8$; (*f*) $(x-x_j)/D = 26.1$, $T = 29.1$; (*g*) $(x-x_j)/D = 31.6$, $T = 34.1$; (*h*) $(x-x_j)/D = 35.8$, $T = 37.5$; (*i*) $(x-x_j)/D = 42.7$, $T = 43.1$. white line, $\langle I \rangle = 0.5$.

attributed to the irregularly fluctuating velocity, u_T' and u_N', rather than the difference between the turbulent and non-turbulent velocity, $u_{ET}-u_{EN}$. On the other hand, in the trailing edge since the variation of an instantaneous velocity with time is less clear than that in the leading edge (Ichimiya, et al., 2011), even if the edge position changes in each ensemble, the velocity difference, $u_{ET}-u_{EN}$, is small. This fact was actually confirmed from the variation of $<u>(t)$, $u_{ET}(t)$ and $u_{EN}(t)$ with T.

The thickness of the above interfaces with surrounding non-turbulent fluid has been reported to extend from the Kolmogorov scale to the Taylor microscale also in a free-shear flow or boundary layer (Rotta, 1962)(Pope, 2000)(Bisset, et al, 2002)(Westerweel, et al., 2005)(da Silva and Taveira, 2010)(Holzner and Lüthi, 2011)(da Silva, et al., 2011)(Semin, et al., 2011). In this turbulent patch, the order of the Kolmogorov scale was estimated as approximately 0.1 mm. Therefore, the thickness of the present leading and trailing edges may be regarded as of the same order. The estimation is obtained from the turbulent energy dissipation rate based on Taylor's evaluation $\varepsilon \sim u_0^3 / l_0$, where u_0 and l_0 mean the velocity and length scales of the large eddy, respectively. Both scales were calculated in the turbulent patch range where the intermittency factor exceeds 0.95. In the range, the difference of the instantaneous and time-averaged velocities, i.e., the fluctuating velocity was obtained first, then its root mean square value was used as u_0. As the length scale of the large eddy, the integration time scale based on the autocorrelation coefficient of the fluctuating velocity was multiplied by the time-averaged velocity there.

Figure 5 shows contour maps of the rms value of the fluctuating velocity on a cross section perpendicular to the pipe axis ($r-\theta$ plane). They were drawn at the maximum fluctuating velocity time in the whole (T, y, θ) position in each $(x-x_j)/D$. Although the half circumferential range $0° \leqq \theta \leqq 180°$ (right half of each figure) was measured except for $(x-x_j)/D = 9.4$ (Fig. 5(c)), the maps are made for the whole circumferential range by drawing the left half symmetrically. The white lines in Fig. 5 depict the half-intermittency. As the cross section is totally occupied by the turbulent patch in the region of $26.1 \leqq (x-x_j)/D$ (Fig. 5(f)~(i)), the white lines are not shown there. The fluctuating velocity is maximum at the symmetrical position, $\theta = 0°$, at $(x-x_j)/D = 2.5$ and 3.5 (Fig. 5(a) and (b)), though it is maximum at the non-symmetrical position at $(x-x_j)/D = 9.4$, 14.9 and 19.2 (Fig. 5(c), (d) and (e)). During this downstream progress from $(x-x_j)/D = 9.4$ to 19.2, the large fluctuation position shifts along the pipe periphery toward

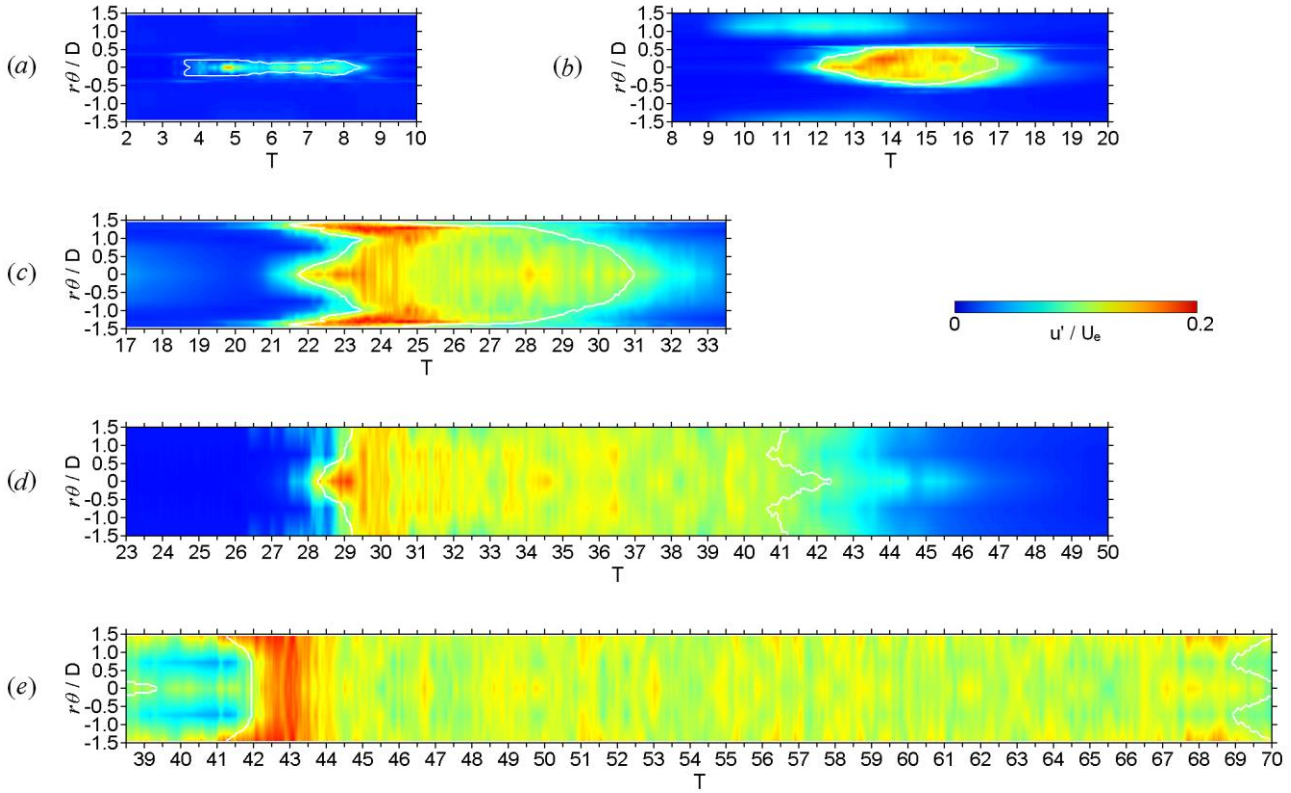

Fig. 6 Contour maps of fluctuating velocity on concentric cylindrical plane. (a) $(x-x_j)/D = 2.5$, $y/a = 0.07$; (b) $(x-x_j)/D = 9.4$, $y/a = 0.05$; (c) $(x-x_j)/D = 19.2$, $y/a = 0.07$; (d) $(x-x_j)/D = 26.1$, $y/a = 0.04$; (e) $(x-x_j)/D = 42.7$, $y/a = 0.07$.white line, $<I> = 0.5$.

180°. The fact that the fluctuating velocity is large near the circumferential edge as well as the axial edge means that the action which entrains the non-turbulent fluid within the boundary layer makes the fluid so turbulent, when the patch spreads in the circumferential direction. The relationship between the entrainment and growth of the patch is discussed in §3.2, though only in the axial direction. In the region 26.1 $\leqq (x-x_j)/D$ (Fig. 5(f)~(i)), the circumferential variation of the fluctuating velocity is small.

Figure 6 shows contour maps of the rms value of the fluctuating velocity in plane views of five typical stations. They were drawn at the height y of the maximum fluctuating velocity time in the whole (T, y, θ) position in each $(x-x_j)/D$. The white lines in Fig. 6 show the half-intermittency. In the region 19.2 $\leqq (x-x_j)/D$ (Fig. 6(c), (d) and (e)), the fluctuating velocity just inside the leading edge is large. At $(x-x_j)/D$ = 19.2 (Fig. 6(c)), the circumferential position of large fluctuating velocity is not around the symmetrical position, θ = 0°, but near the circumferential edge. In the flat-plate turbulent spot the fluctuating velocity is large not on its centerline but near the spanwise edge (Glezer, et al., 1989). The spanwise growth mechanism of the spot may be explained as the breakdown of a wave near the spanwise edge (Glezer, et al., 1989). Examining the presence of the wave in and out of the circumferential edge in the present turbulent patch is a problem for future study.

3.2 Growth mechanism of turbulent patch

In this section, the mechanism of the growth of the turbulent patch is discussed with observations of the axial entrainment of the non-turbulent fluid through the leading and trailing edges. First, as Wygnanski et al. carried out for both the turbulent slugs in the HP flow (Wygnanski and Champagne, 1973) and the turbulent spots in a flat-plate boundary layer (Wygnanski, et al., 1976), the relative streamlines to the leading and trailing edges are drawn and fluid movement through the edges is considered. Here, Stokes' stream function is calculated in the diametrical planes of θ = 0°. For example, the stream function relative to the leading edge is given by the following equation (Wygnanski and Champagne, 1973):

$$\psi_l(T,r)=\int_0^r r'\left\{\,[U(r')+<u>(T,r')]-[U(r')+<u>(r')]_l\,\right\}dr'=\int_0^r r'[<u>(T,r')-<u>(r')_l]dr'$$

$$=\int_y^a (a-y')[<u>(T,y')-<u>(y')_l]dy' \tag{9}$$

That is, the integration was performed with a transformation of a radial distance from the pipe axis, r, to the height from the pipe wall, $y = a-r$. The velocity at the leading edge, $[U(r) + \langle u\rangle(r)]_l$ is an ensemble-averaged velocity at respective (T, r) positions in the leading edge. Since in the leading edge, if the r is given the T is decided automatically, the leading edge velocity is a function of r (or y) alone. The streamlines relative to the trailing edge are obtained similarly. In the axial station $(x-x_j)/D$ = 9.4 among two stations in Fig. 7, the axisymmetry has not been established since the turbulent patch has not spread in the whole periphery there as seen in Fig. 5(c). Though the Stokes' stream function only exists in an axisymmetric flows, the stream function was obtained there for reference. Farther downstream, station $(x-x_j)/D$ = 26.1 in Fig. 7, can be considered as sufficient axisymmetry as seen in Fig. 5(f).

In Fig. 7 the relative streamlines with respect to the leading and trailing edges are shown at two axial stations; one is $(x-x_j)/D$ = 9.4, representative of the turbulent spot type in a flat-plate boundary layer; the other is $(x-x_j)/D$ = 26.1, representative of the turbulent slug type. Since at $(x-x_j)/D$ = 9.4 (Fig. 7(a) and (b)), the height of $< I >$ = 0.5 did not reach the pipe axis, the relative streamlines were drawn in the region of 0 $\leqq y/a \leqq$ 0.5. At $(x-x_j)/D$ = 26.1 (Fig. 7(c) and (d)), the streamlines were drawn in the range from the pipe wall to the axis. As the streamlines, contour lines of the stream functions, ψ_l (Fig. 7(a) and (c)), or ψ_t (Fig. 7(b) and (d)), normalized by $U_e a^2$, were drawn every other 0.002. The values are indicated in blue numerals in Fig. 7. The arrow showed the flow direction. Moreover, the leading and trailing edges are shown in red lines, and the edges of the boundary layer determined from the ensemble-averaged velocity at respective T are shown in green lines. In every figure, at the leading edge, fluid flows into the turbulent patch from the downstream outside. On the other hand, fluid flows from the upstream outside at the trailing edge. The fact that the fluid outside the patch flows into it through both edges can be seen also in the turbulent slug in the HP flow (Wygnanski and Champagne, 1973) and the turbulent spot in the flat-plate boundary layer (Wygnanski, et al., 1976). In

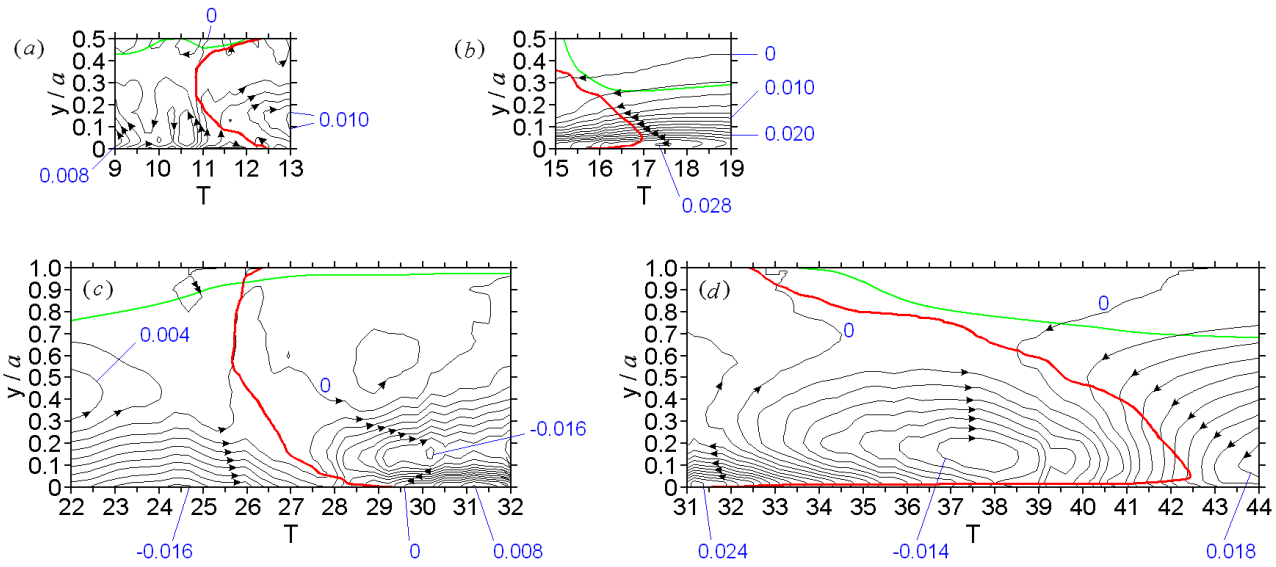

Fig. 7 Streamline relative to interfaces. (*a*) $(x-x_j)/D = 9.4$, leading edge; (*b*) $(x-x_j)/D = 9.4$, trailing edge; (*c*) $(x-x_j)/D = 26.1$, leading edge; (*d*) $(x-x_j)/D = 26.1$, trailing edge; red line, $<I> = 0.5$; green line, boundary layer thickness.

the turbulent slug the relative streamlines were parallel to the pipe wall also in the leading and trailing edges (Wygnanski and Champagne, 1973). On the other hand, in the leading edge in the turbulent spot there is an overhang part which rose up from the wall. The relative streamlines were parallel to the wall undersurface but slanted toward the wall from the upper surface of the overhang part (Wygnanski, et al., 1976). At the trailing edge the relative streamlines were parallel with the wall (Wygnanski, et al., 1976).

We here examine in detail the inflow direction of the relative streamline. In the leading edge of $(x-x_j)/D = 9.4$ (Fig. 7(*a*)), in the overhang part, $y/a \leqq 0.2$, the streamlines rise upward (from the wall toward the pipe center axis). Thus, the fluid within the boundary layer having a mean vorticity, $\partial(U + <u>)/\partial y$, flows into the patch. The streamline does not flow in from the upper surface of the overhang part, contrary to the turbulent spot. Though a pressure gradient or a wall curvature might reflect the difference, the detailed discussion should be based on the equations in cylindrical coordinates. In this paper, the discussion is limited for obtaining the similarities and differences between the present turbulent patch and turbulent slug or turbulent spot. At the trailing edge (Fig. 7(*b*)), the streamlines are flowing from upstream parallel to the wall through the slanted interface in $0.05 \leqq y/a$, the same as a turbulent slug or turbulent spot. Although in $y/a \leqq 0.25$, the fluid which has the mean vorticity within the boundary layer is flowing in like the leading edge, in $0.25 < y/a$ fluid without the mean vorticity outside the boundary layer is flowing in, the same as the turbulent spot.

In the leading edge at $(x-x_j)/D = 26.1$ (Fig. 7(*c*)), the fluid which has mean vorticity flows in only $y/a < 0.2$ under the overhang part from downstream, the same as the turbulent slug and the turbulent spot. Until near the trailing edge (Fig. 7(*d*)), the fluid with the mean vorticity within the boundary layer approaches from upstream parallel to the wall, the same as the trailing edge of $(x-x_j)/D = 9.4$ (Fig. 7(*b*)). However, in just the trailing edge here, the fluid flows through the slanted surface of $0.1 \leqq y/a$, from the pipe center to the wall direction. This condition differs from the turbulent slug or the turbulent spot with relative streamlines parallel to the wall. Furthermore, although it is the same as the trailing edge of $(x-x_j)/D = 9.4$ (Fig. 7(*b*)) that fluid without the mean vorticity outside the boundary layer flows in around the pipe center, here the fluid flows downward (toward the wall of $\theta = 0°$). Values of $\psi/(U_e a^2)$ which flows into the patch are more widespread in the trailing edge than the leading edge; thus the flow comes more in the trailing edge within the same radial range. For this reason, the distance between the maximum fluctuation position and the trailing edge increases as in Fig. 3.

Next, we examine whether the fluid entrained from outside through the leading and trailing edges is turbulent or non-turbulent. Therefore, the ensemble-averaged velocity conditioned by turbulent/non-turbulent is utilized. First, from the turbulent or non-turbulent conditional ensemble-averaged velocity, Eq. (3) or (4), the non-conditional one is subtracted. These differences are plotted in Fig. 8 at the representative five stations. From the distributions, the relative velocity of the turbulent or non-turbulent fluids with respect to the turbulent patch can be estimated. Since the

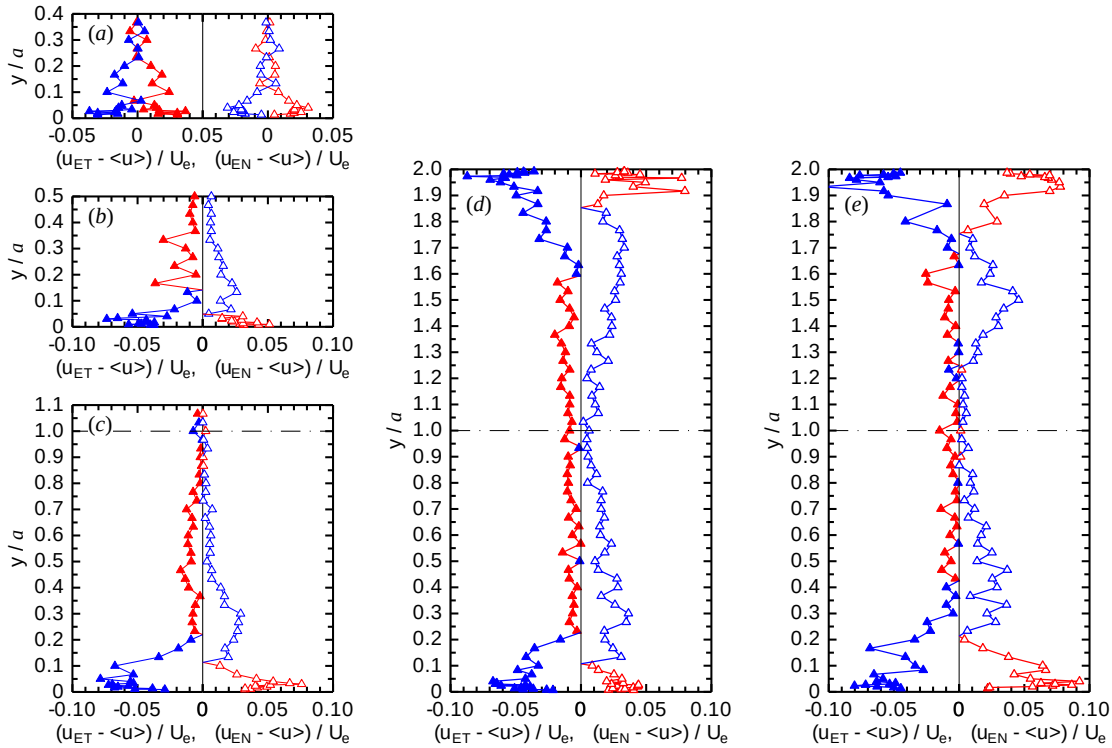

Fig. 8 Radial distribution of conditionally-averaged relative velocity on leading (left) and trailing (right) edges. (*a*) $(x-x_j)/D = 2.5$; (*b*) $(x-x_j)/D = 9.4$; (*c*) $(x-x_j)/D = 19.2$; (*d*) $(x-x_j)/D = 26.1$; (*e*) $(x-x_j)/D = 42.7$; closed symbols, leading edge; open symbols, trailing edge; red, u_{ET} - <*u*>; blue, u_{EN} - <*u*>.

intermittency factor is a half at the leading and trailing edges, the following relation holds among the relative velocities:

$$u_{ET}(t) - < u >(t) = -[u_{EN}(t) - < u >(t)] \tag{10}$$

The left-hand side and the inside of the bracket in the right-hand side of Eq. (10) are shown with red and blue colors in Fig. 8, respectively. At both the leading and trailing edges in $(x-x_j)/D = 2.5$ (Fig. 8(*a*)), the red and blue symbols are very symmetric with respect to zero, thus verifying Eq. (10). From the relative streamlines in Fig. 7, the fluid outside of the turbulent patch is shown to flow into the patch in the upstream and downstream directions at the leading and trailing edges, respectively. Therefore, in Fig. 8(*b*)~(*e*), at the leading edge only negative values, i.e., the velocity toward upstream are shown; on the other hand, at the trailing edge only positive values are indicated, i.e., the velocity in the downstream direction.

At $(x-x_j)/D = 9.4$ (Fig. 8(*b*)) whose relative streamlines were shown in Fig. 7(*a*) and (*b*), in $y/a < 0.15$ of the leading edge the non-turbulent velocity is negative, and the fact that it flows into the leading edge from the outside of the patch through the overhang part undersurface is confirmed. In $0.05 \leqq y/a$ of the trailing edge, the non-turbulent velocity is positive, and proves that it flows in from the outside of the patch through the slope of the trailing edge. In this way, since the sign of the relative velocity of non-turbulent fluid corresponds with the direction of the relative streamlines, movements of this non-turbulent fluid is discussed. In $0.25 < y/a$ of the trailing edge, where the fluid which does not have the mean vorticity outside the boundary layer was flowing in Fig. 7(*b*), the non-turbulent fluid is flowing in, although the relative velocity is small. Moreover, at $(x-x_j)/D = 26.1$ (Fig. 8(*d*)), where the relative streamlines were shown in Figs. 7(*c*) and (*d*), in $y/a < 0.2$ of the leading edge, it is confirmed that the non-turbulent fluid is flowing in from the outside through undersurface of the overhang part. In $0.1 \leqq y/a$ of the trailing edge, the fact that the non-turbulent fluid is flowing in from the outside through the upper surface is confirmed. Moreover, in Fig. 7(*d*), where the non-turbulent fluid which does not have the mean vorticity outside the boundary layer was flowing in near the pipe center, here the non-turbulent fluid is flowing in, though the velocity is small. Also, in other $(x-x_j)/D$, near the wall in the leading edge, the non-turbulent fluid outside of the patch flows in; on the other hand, slightly away from the wall in the trailing edge, the non-turbulent fluid outside the patch flows in. In this way, at the leading edge near the wall and

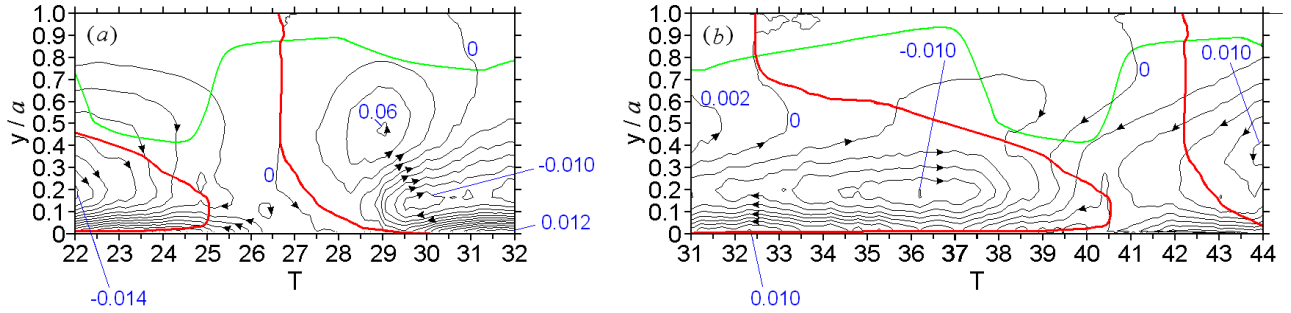

Fig. 9 Streamlines relative to leading (*a*) and trailing (*b*) edges. $(x-x_j)/D = 26.1$, $t_{j2} = 0.3$ s. red line, $<I> = 0.5$; green line, boundary layer thickness.

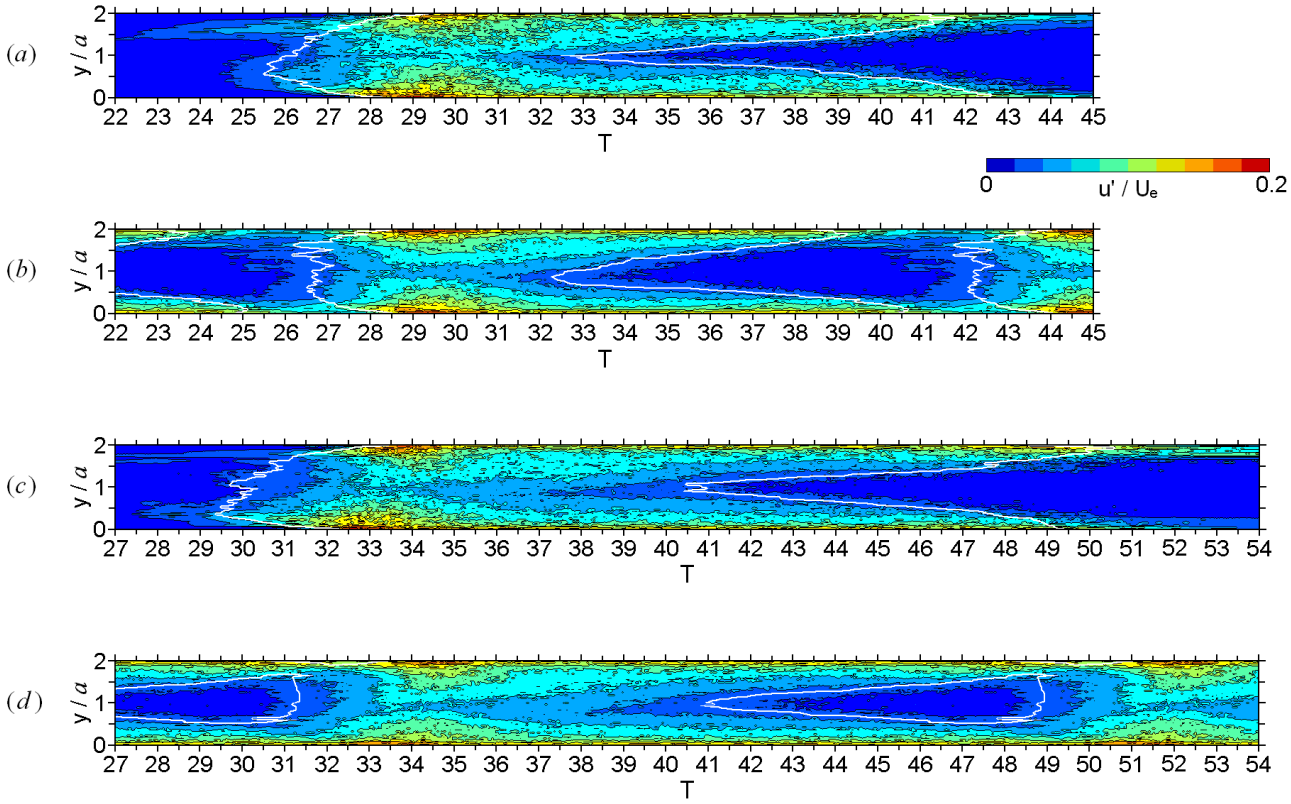

Fig. 10 Contour maps of fluctuating velocity on diametrical plane. (*a*) $(x-x_j)/D = 26.1$, $t_{j2} = 0.7$ s; (*b*) $(x-x_j)/D = 26.1$, $t_{j2} = 0.3$ s ; (*c*) $(x-x_j)/D = 31.6$, $t_{j2} = 0.7$ s; (*d*) $(x-x_j)/D = 31.6$, $t_{j2} = 0.3$ s. white line, $<I> = 0.5$.

the trailing edge slightly away from the wall, respectively, the entrainment of the non-turbulent fluid contributes to the growth of the patch. In addition, at $\theta = 0°$ and 180° near the wall, although the values are scattered, a point of inflection exists in the ensemble-averaged velocity distribution as described in § 3.1. The distortion of the distribution profile by the point of inflection is the maximum and minimum in the turbulent average, $U + u_{ET}$, and the non-turbulent average, $U + u_{EN}$, respectively. In this way, since the degree of the distortion of u_{ET} and u_{EN} is different, the scatter is large near the wall.

In order to confirm that the entrainment of the non-turbulent fluid and its increasing turbulence contributes to the growth of the turbulent patch, the entrainment is decreased intentionally. If the interval between the trailing edge of a certain patch and the leading edge of the next patch is narrowed, the non-turbulent fluid in the narrow space may be forced toward both patches, and as a result the fluid entrained into each patch will decrease. As mentioned before, although the jet non-injection duration, t_{j2}, was set to 0.7 seconds in the region of $26.1 \leqq (x-x_j)/D$, here it is set instead to 0.3 seconds. With this shorter interval, although at $(x-x_j)/D = 26.1$, the two patches had not merged, they did so at $31.6 \leqq (x-x_j)/D$; the result of $(x-x_j)/D = 26.1$ is mainly described.

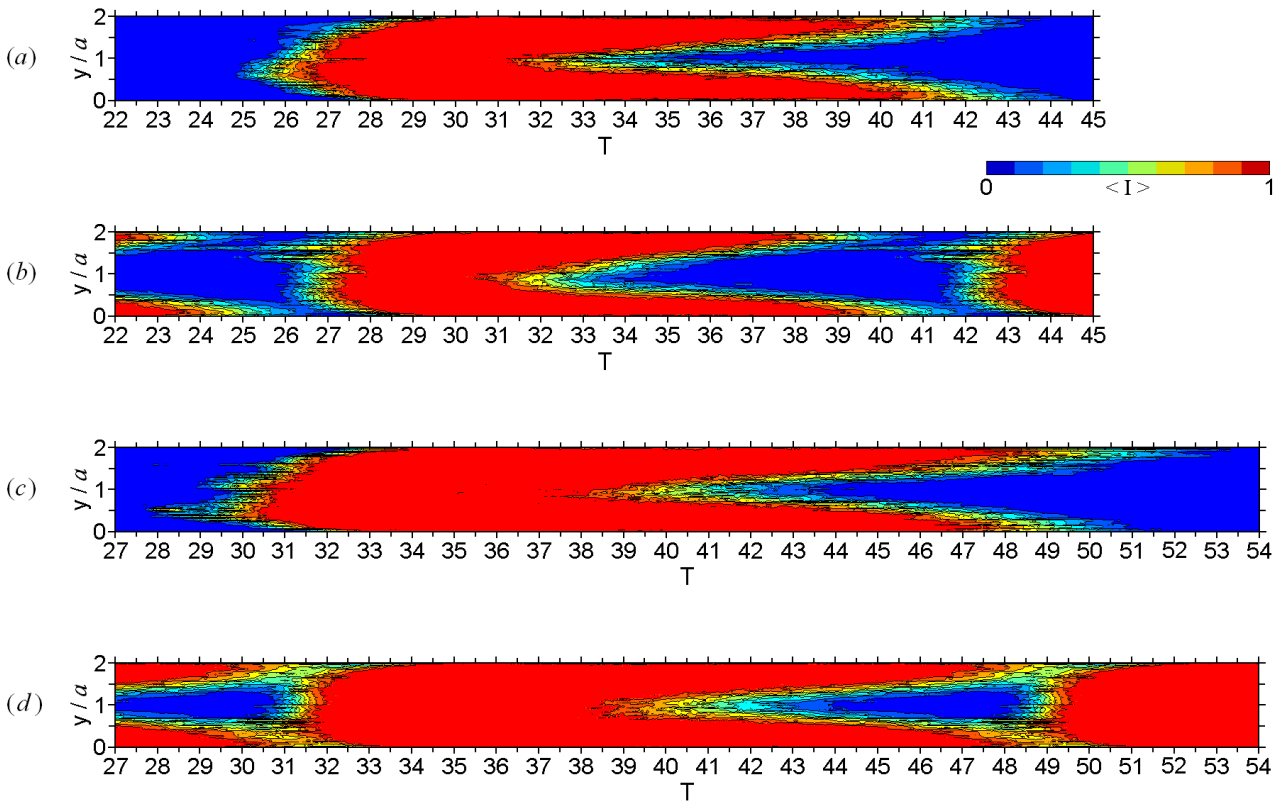

Fig. 11 Intermittency contour maps on diametrical plane. (*a*) $(x-x_j)/D$ = 26.1, t_{j2} = 0.7 s; (*b*) $(x-x_j)/D$ = 26.1, t_{j2} = 0.3 s; (*c*) $(x-x_j)/D$ = 31.6, t_{j2} = 0.7 s; (*d*) $(x-x_j)/D$ = 31.6, t_{j2} = 0.3 s.

Figure 9 shows the relative streamlines. Compared with the streamlines with the longer interval, 0.7 seconds (Fig. 7(*c*) and (*d*)), the streamlines do not enter through the leading edge, and the number of streamlines taken in at the trailing edge decreased considerably. Therefore, the flow entrained within the patch decreased as expected.

The entrained non-turbulent fluid will not become fully turbulent due to the reduced flow rate. To confirm this assumption, the contour maps of the irregularly fluctuating velocity on the diametrical plane at $(x-x_j)/D$ = 26.1 and 31.6 are shown in Fig. 10. Although the contour maps with the longer interval were also shown in Fig. 2(*f*) and (*g*), to compare with the shorter interval, a ratio of the abscissa and the ordinate of the maps was changed and shown again in Fig. 10(*a*) and (*c*). At both stations, the fluctuating velocities are smaller with the shorter interval (Fig. 10(*b*) and (*d*)) on the whole, thus confirming that the fluid becomes less turbulent, since there little non-turbulent fluid is entrained.

Here we finally discuss the effect of the reduced entrainment of the non-turbulent fluid of the turbulent patch. Figure 11 shows the contour maps of the intermittency factor on the diametrical plane at $(x-x_j)/D$ = 26.1 and 31.6. The axial length of the patch with the 0.3-second interval (Fig. 11(*b*) and (*d*)) is shorter. As a guide to the patch's length at $(x-x_j)/D$ = 26.1 (Fig. 11(*a*) and (*b*)), four positions are selected; the most downstream leading edge, T_l, the leading edge on the pipe axis (y/a = 1), T_1, the trailing edge on the pipe axis, T_2, and the most upstream trailing edge, T_t. They (T_l, T_1, T_2, T_t) are (25.5, 26.3, 32.4, 42.6) and (26.2, 26.6, 32.2, 40.6) with the longer (Fig. 11(*a*)) or shorter (Fig. 11(*b*)) intervals, respectively. The distance between T_2 and T_t is shorter with the shorter interval. Less non-turbulent fluid entrainment with the shorter interval, especially from the slope of the trailing edge as mentioned above, contributes to the shrinkage. The above result confirms that the non-turbulent fluid entrainment from the leading edge and especially from the trailing edge is the main factor in the axial growth of the turbulent patch. Downstream, at $(x-x_j)/D$ = 31.6 with shorter interval (Fig. 11(*d*)), the length is prohibited, although adjacent turbulent patches are merging. That is, by narrowing the interval between two turbulent patches, the non-turbulent fluid entrainment into the patch decreases. This prohibits the axial growth of the patch and decreases the fluctuating velocity within it.

4. Conclusions

An isolated turbulent patch was generated by a periodical jet injection into an inlet region of a circle pipe. The

fluctuating velocities within the patch were measured in the inlet region, and the following conclusions were obtained.

(1) The irregularly fluctuating velocity from the ensemble-averaged velocity becomes a maximum four times of the normalized time inside from the most downstream leading edge in the axial direction, and in the circumferential position out of the axis of symmetry. These features are the same as the flat-plate turbulent spot. This means that what causes the outside non-turbulent fluid entrainment and makes it fully turbulent has been triggered.

(2) The non-turbulent fluid entrainment through the leading and the trailing edges leading to full turbulence makes for the axial growth of the turbulent patch. When the entrainment is little, the fluctuating velocity within the patch is small and the axial growth becomes weak. The non-turbulent fluid entrainment is larger in the trailing edge than the leading edge. Therefore, the distance between the maximum fluctuating position and the trailing edge increases significantly downstream. This increase is expressed by an exponential or a power function, though the degree of approximation of the power function is higher.

(3) While the form of the turbulent patch is flat-plate turbulent spot type, only the non-turbulent fluid with a mean vorticity near the pipe wall is entrained upward from the leading edge, contrary to the turbulent spot. At the trailing edge, both the non-turbulent fluid with the mean vorticity near the wall and it without the mean vorticity near the pipe axis are entrained, the same as the turbulent spot.

(4) When the turbulent patch proceeds downstream and becomes turbulent-slug type, at the leading edge the non-turbulent fluid entrainment with the mean vorticity is only near the wall, contrary to the turbulent slug or the turbulent spot. At the trailing edge, the non-turbulent fluid with the mean vorticity near the wall and without the mean vorticity away from the wall move in the downward direction, contrary to the turbulent slug or the turbulent spot.

Acknowledgments

The authors appreciate the kind instruction and constant encouragement of Prof. I. Nakamura, Nagoya University. The generous assistance of Messrs. H. Nishida, M. Funaki, H. Ohno and K. Satou of the University of Tokushima is also gratefully acknowledged.

References

Bisset, D. K., Hunt, J. C. R. and Rogers, M. M., The turbulent/non-turbulent interface bounding a far wake, Journal of Fluid Mechanics, Vol. 451 (2002), pp. 383–410.

da Silva, C. B. and Taveira, R., The thickness of the turbulent/nonturbulent interface is equal to the radius of the large vorticity structures near the edge of the shear layer, The Physics of Fluids, Vol. 22, Issue 12, 121702 (2010).

da Silva, C. B., dos Reis, R. J. N. and Pereira, J. C. F., The intense vorticity structures near the turbulent/non-turbulent interface in a jet, Journal of Fluid Mechanics, Vol. 685 (2011), pp. 165–190.

Durst, F. and Ünsal, B., Forced laminar-to-turbulent transition of pipe flows, Journal of Fluid Mechanics, Vol. 560 (2006), pp. 449–464.

Eckhardt, B., Turbulence transition in pipe flow: Some open questions, Nonlinearity, Vol. 21, No. 1 (2008), pp. T1–T11.

Eckhardt, B., Schneider, T. M., Hof, B. and Westerweel, J., Turbulence transition in pipe flow, Annual Review of Fluid Mechanics, Vol. 39 (2007), pp. 447–468.

Eliahou, S., Tumin, A. and Wygnanski, I., Laminar–turbulent transition in Poiseuille pipe flow subjected to periodic perturbation emanating from the wall, Journal of Fluid Mechanics, Vol. 361 (1998), pp. 333–349.

Glezer, A., Katz, Y. and Wygnanski, I., On the breakdown of the wave packet trailing a turbulent spot in a laminar boundary layer, Journal of Fluid Mechanics, Vol. 198 (1989), pp. 1–26.

Han, G., Tumin, A. and Wygnanski, I., Laminar–turbulent transition in Poiseuille pipe flow subjected to periodic perturbation emanating from the wall. Part 2. Late stage of transition, Journal of Fluid Mechanics, Vol. 419 (2000), pp. 1–27.

Holzner, M. and Lüthi, B., Laminar superlayer at the turbulence boundary, Physical Review Letters, Vol. 106, Issue. 13, 134503 (2011).

Ichimiya, M., Abe, T., Fukutomi, J. and Kondo, M., Laminar-turbulent transition of a boundary layer induced by a single roughness element in an inlet region of a circular pipe flow (Developing process of a stationary turbulent

region), Transactions of the Japan Society of Mechanical Engineers, B, Vol. 73, No. 725 (2007), pp. 154–161. (in Japanese)

Ichimiya, M., Fujimura, H. and Tamatani, J., Laminar-turbulent transition of an inlet boundary layer in a circular pipe induced by periodic ejection (Condition for generating an isolated turbulent patch), Journal of Fluid Science and Technology, Vol. 6, No. 6 (2011), pp. 902–915.

Ichimiya, M., Matsudaira, H., Fujimura, H. and Ohno, H., Laminar-turbulent transition of an inlet boundary layer in a circular pipe induced by periodic injection (Shape of isolated turbulent patches and their growth), Journal of Fluid Science and Technology, Vol. 8, No. 3 (2013), pp. 436–451.

Kerswell, R. R., Recent progress in understanding the transition to turbulence in a pipe, Nonlinearity, Vol. 18, No. 6 (2005), pp. R17–R44.

Makita, H. and Nishizawa, A., Interaction between two horizontally displaced turbulent spots, Transactions of the Japan Society of Mechanical Engineers, Series B, Vol. 64, No. 627 (1998), pp. 3682–3689. (in Japanese)

Nishi, M, Ünsal, B., Durst, F. and Biswas, G., Laminar-to-turbulent transition of pipe flows through puffs and slugs, Journal of Fluid Mechanics, Vol. 614 (2008), pp. 425–446.

Pope, S. B., Turbulent Flows (2000), p. 171, Cambridge University Press.

Rotta, J. C., Turbulent boundary layers in incompressible flow, Ferri, A., Kuchemann, D. and Sterne, L. H. G. ed., Progress in Aeronautical Sciences (1962), pp. 86, Pergamon Press.

Semin, N. V., Golub, V. V., Elsinga, G. E. and Westerweel, J., Laminar superlayer in a turbulent boundary layer, Technical Physics Letters, Vol. 37, No. 12 (2011), pp. 1154–1157.

Westerweel, J., Fukushima, C., Pedersen, J. M. and Hunt, J. C. R., Mechanics of the turbulent- nonturbulent interface of a jet, Physical Review Letters, Vol. 95, Issue. 17, 174501 (2005).

Willis, A. P., Peixinho, J., Kerswell, R. R. and Mullin, T., Experimental and theoretical progress in pipe flow transition, Philosophical Transactions of the Royal Society, A, Vol. 366 (2008), pp. 2671–2684.

Wygnanski, I. J. and Champagne, F. H., On transition in a pipe. Part 1. The origin of puffs and slugs and the flow in a turbulent slug, Journal of Fluid Mechanics, Vol. 59, Pt. 2 (1973), pp. 281–335.

Wygnanski, I., Sokolov, M. and Friedman, D., On a turbulent ‘spot’ in a laminar boundary layer, Journal of Fluid Mechanics, Vol. 78, Pt. 4 (1976), pp. 785–819.